Volume 66. Number 14. December 2006

JOURNAL OF Neurobiology

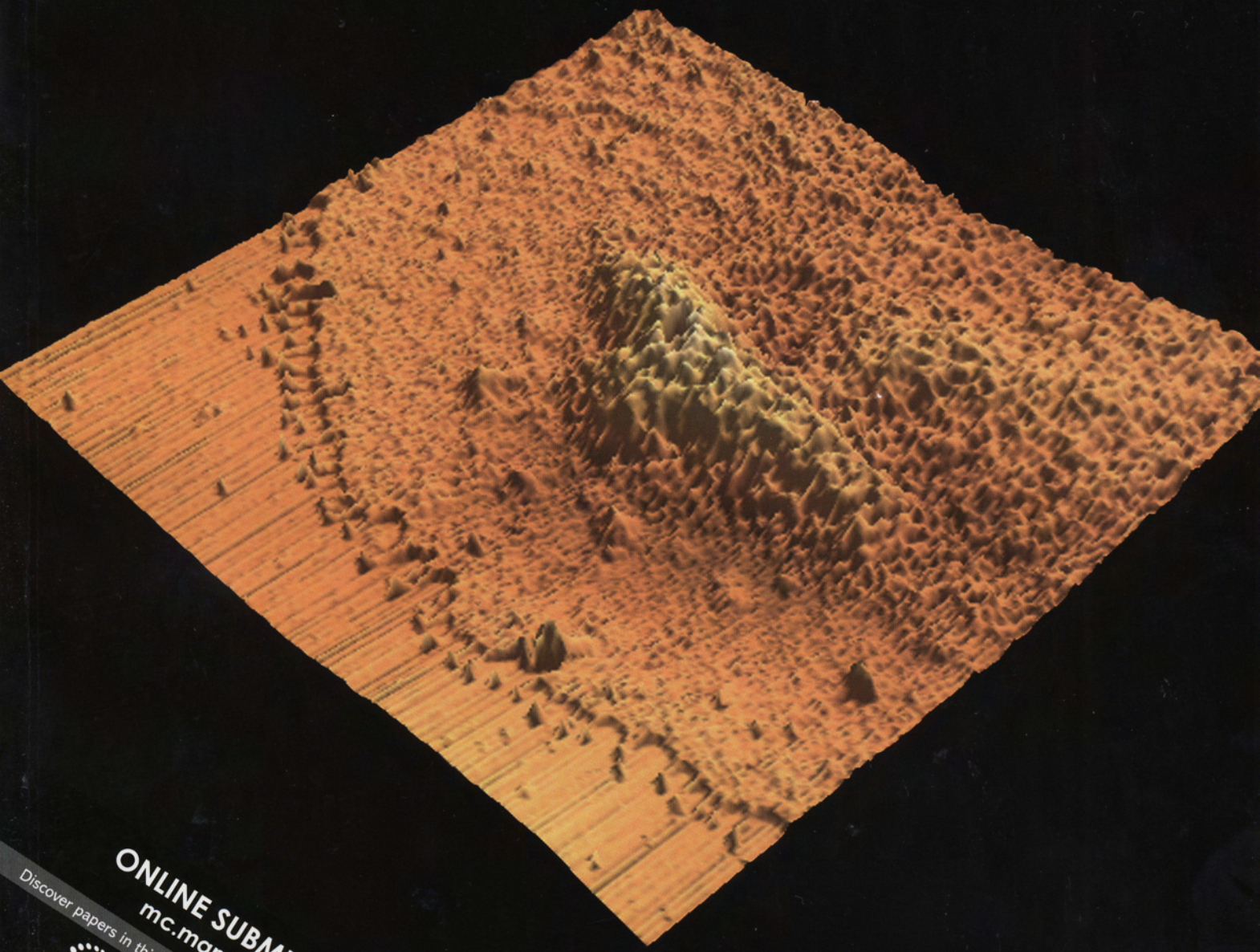

High-Resolution Analysis of Neuronal Growth Cone Morphology by Comparative Atomic Force and Optical Microscopy

Emilie L. Grzywa,[1] Aih Cheun Lee,[2] Gil U. Lee,[1,3] Daniel M. Suter,[2,3]

[1] School of Chemical Engineering, Purdue University, West Lafayette, Indiana 47907-2100

[2] Department of Biological Sciences, Purdue University, West Lafayette, Indiana 47907-2054

[3] Bindley Bioscience Center, Purdue University, West Lafayette, Indiana 47907

Received 12 May 2006; revised 13 June 2006; accepted 23 June 2006

ABSTRACT: **Neuronal growth cones are motile sensory structures at the tip of axons, transducing guidance information into directional movements towards target cells. The morphology and dynamics of neuronal growth cones have been well characterized with optical techniques; however, very little quantitative information is available on the three-dimensional structure and mechanical properties of distinct subregions. In the present study, we imaged the large *Aplysia* growth cones after chemical fixation with the atomic force microscope (AFM) and directly compared our data with images acquired by light microscopy methods. Constant force imaging in contact mode in combination with force-distant measurements revealed an average height of 200 nm for the peripheral (P) domain, 800 nm for the transition (T) zone, and 1200 nm for the central (C) domain, respectively. The AFM images show that the filopodial F-actin bundles are stiffer than surrounding F-actin networks. Enlarged filopodia tips are 60 nm higher than the corresponding shafts. Measurements of the mechanical properties of the specific growth cone regions with the AFM revealed that the T zone is stiffer than the P and the C domain. Direct comparison of AFM and optical data acquired by differential interference contrast and fluorescence microscopy revealed a good correlation between these imaging methods. However, the AFM provides height and volume information at higher resolution than fluorescence methods frequently used to estimate the volume of cellular compartments. These findings suggest that AFM measurements on live growth cones will provide a quantitative understanding of how proteins can move between different growth cone regions.** J Neurobiol 66: 1529–1543, 2006

Keywords: **atomic force microscopy; growth cone; cytoskeleton; filopodia; volume measurement**

INTRODUCTION

The neuronal growth cone is the motile sensory structure at the end of the axon that detects extracellular guidance cues and integrates this information into directional movement towards the target cell. While the role of guidance molecules (Dickson, 2002), underlying signaling pathways (Song and Poo, 2001; Huber et al., 2003), and both the F-actin and microtubule cytoskeletons (Dent and Gertler, 2003) are well established for growth cone movements, relatively little is known about the three-dimensional structures

Correspondence to: Dr. D. Suter (dsuter@purdue.edu) and Dr. G. Lee (gl@ecn.purdue.edu).

Contract grant sponsor: NIH; contract grant number: R01 NS049233.

Contract grant sponsor: Bindley Bioscience Center at Purdue University.

Contract grant sponsor: NASA Institute for Nanoelectronics and Computing; contract grant number: NASA NCC 2-1363.

Published online 20 October 2006 in Wiley InterScience (www.interscience.wiley.com).
DOI 10.1002/neu.20318

and mechanical properties of these dynamic neuronal structures and how signaling pathways control the cytoskeleton.

Aplysia bag cell neuronal growth cones in culture exhibit a large fan-like shape with distinct cytoplasmic regions (Forscher and Smith, 1988). The peripheral (P) domain consists of flat lamellipodia that are subdivided by radial filopodial F-actin bundles. The central (C) domain mainly contains microtubules and vesicles of various sizes. High resolution video-enhanced differential interference contrast (DIC) microscopy has been used to visualize the morphological changes during the different steps of neurite outgrowth and growth cone turning events (Goldberg and Burmeister, 1986; Lin and Forscher, 1993; Suter et al., 1998). Because of their large size, *Aplysia* growth cones are an excellent model system for biophysical studies addressing receptor-cytoskeletal coupling (Suter et al., 1998) as well as for the high resolution imaging and analysis of F-actin and microtubule dynamics (Schaefer et al., 2002; Zhang et al., 2003).

The atomic force microscope (AFM) is a powerful instrument for imaging, manipulating, and force mapping at the nanometer (nm) and nano-Newton (nN) scale. Shortly after its invention (Binnig et al., 1986), researchers started to use AFM to probe a variety of biological samples from single proteins to cells (Engel et al., 1999; Dvorak, 2003; Santos and Castanho, 2004). AFM has been used to visualize a variety of cell types, including glial cells, macrophages, acinar cells, fibroblasts, endothelial cells, neurons, both live and fixed (e.g. Henderson et al., 1992; Rotsch et al., 1997; Schneider et al., 1997; Braet et al., 2001; McNally and Borgens, 2004; Pesen and Hoh, 2005). A small number of AFM studies investigated neurons, focusing on the cell body, axon, and synaptic vesicle structure (Parpura et al., 1993; Lal et al., 1995; Tojima et al., 2000; McNally and Borgens, 2004; Ricci et al., 2004; McNally et al., 2005); however, there was a limited attempt to study neuronal growth cones in detail.

Therefore, we employed AFM imaging of chemically fixed *Aplysia* growth cones in contact mode to determine the topography of various growth cone regions. We provide the first comprehensive three-dimensional analysis of these regions as well as measurements of their mechanical properties. Furthermore, the AFM height images have been directly compared with DIC images, cytoskeletal labeling, and volume measurements made with conventional fluorescence microscopy. Interestingly, the AFM measurements were found to highlight some of the cytoskeletal structures of the growth cone and provided volume results similar to fluorescence microscopy, but at a much higher resolution and better signal-to-noise ratio. Thus, AFM imaging is an excellent method to map growth cone topography and mechanics, providing important information for evaluating models of protein dynamics related to growth cone function.

METHODS

Aplysia Bag Cell Neuronal Culture

Aplysia bag cell neurons were cultured on polylysine-coated #1 glass coverslips in L15 medium (Invitrogen/GIBCO, Carlsbad, CA) supplemented with artificial seawater (ASW), as previously described (Forscher and Smith, 1988; Suter et al., 1998). Cells were used for both optical and AFM imaging 1 day after plating.

Fluorescence Labeling and Light Microscopy

F-actin and microtubule labeling of fixed bag cell growth cones was carried out as recently described (Suter et al., 2004). Briefly, bag cell neurons were fixed by rapid exchange of the medium with 3.7% formaldehyde in ASW supplemented with 400 mM sucrose. After fixation for 15 min at room temperature (RT), the cells were permeabilized for 10 min, using 1% triton X-100 in the fixation solution. Cells were then washed three times with phosphate buffered saline (PBS) containing 0.1% triton X-100 (wash solution). For actin filament labeling, Alexa 568-phalloidin (Molecular Probes, Eugene, OR) was incubated at 1 unit/mL in wash solution for 30 min. After three washes the cells were blocked with 5% bovine serum albumin (Sigma, St. Louis, MO) in wash solution for 30 min and incubated with the mouse anti-α-tubulin antibody (ascites, clone B-5-1-2, Sigma) at 1:1000 in blocking solution for 1 h at RT. After three washes, Alexa 488 goat anti-mouse IgG (Molecular Probes) was added at 4 μg/mL in blocking solution for 30 min at RT. The final wash solution was replaced with antifading solution (20 mM *n*-propyl-gallate (Sigma) in 80% glycerol/20% PBS, pH 8.5) before fluorescence inspection.

For fluorescent volume imaging, bag cell neurons were microinjected with 2.5 mg/mL lysine-fixable 3 kDa Texas Red dextran (Molecular Probes) in sterile water using an NK-2 micromanipulator (Eppendorf, Westbury, NY) and a Femtojet microinjection system (Eppendorf). Injection needles with 1-μm-wide tip opening were pulled from borosilicate glass capillaries (1B100F-4, World Precision Instruments, Sarasota, FL) using a PP-830 micropipette puller (Narashige, East Meadow, NY). The cells were allowed to recover for 1 h after dextran injections before chemical fixation was performed as described previously. Fixation solution was then exchanged with ASW before imaging in fluorescence and AFM mode.

Light microscopy images were acquired on a Nikon Eclipse TE2000U inverted microscope (Nikon, Melville, NY) equipped with phase, DIC and fluorescence optics, and Proscan 109 xyz stage control (Prior Scientific, Rockland, MA). The Lambda LS, a 175 W Xenon lamp (Sutter Instrument, Novato, CA), plus the λ-10 filter wheel and shutter control unit (Sutter Instrument) were used for fluorescence illumination. Appropriate FITC and Texas Red filter cubes were selected for imaging of Alexa 488 and Alexa 568/Texas Red fluorescent dyes, respectively. Digital images were acquired with a CoolSNAP HQ cooled CCD camera (Roper Scientific, Tucson, AZ). Microscope illumination, stage, and camera were controlled by Metamorph 6.2 software (Universal Imaging, Molecular Devices, Downingtown, PA).

Atomic Force Microscopy

A commercial AFM (MFP3D AFM, Asylum Research, Santa Barbara, CA) that was integrated with an inverted epifluorescence optical microscope (Eclipse 300, Nikon) was used to study growth cones. Contact mode AFM imaging (Engel et al., 1999) was performed in ASW using commercial Si_3N_4 microfabricated cantilevers that have integrated pyramidal probes with a nominal radius of 20 nm (Olympus, Melville, NY). The radius of curvature of the probes was measured with $SrTiO_3$ crystals (Sheiko et al., 1993). Imaging was performed with "soft" cantilevers that were 0.8 μm thick and 200 μm long. These cantilevers have nominal resonance frequencies and spring constants of 17–24 kHz and 0.06–0.15 N/m, respectively (Green et al., 2004). Before each experiment, the cantilevers were cleaned with ozone, and their spring constant was determined in air using the thermal power spectrum of the cantilevers. The sensitivity of the optical lever detector was determined after imaging the cells by pressing the cantilever against the glass surface. Contact mode imaging was performed at constant force using a feedback loop system. Constant force was applied to the sample resulting in piezo displacements revealing height differences.

For AFM imaging, a glass cover slip with the fixed neurons was mounted on a 10 cm plastic Petri dish using high vacuum grease. The dish was then filled with ASW solution and the cantilever tip was manually lowered to the cell surface. The cells were identified with the inverted optical microscope using a 10× objective and transmitted light. A high resolution scan (5 × 5 μm) of the glass surface near a cell was first made to check if the instrument was functioning properly. Then, the AFM cantilever was positioned near the edge of the growth cone to begin imaging in a closed-loop mode at scan sizes varying between 2 × 2 μm and 90 × 90 μm. The scan rates were adjusted between 0.1 and 1 Hz to keep the scanning speed below 20 μm/s. The feedback force set point was minimized to keep the imaging force on the cell as low as possible, which in practice was found to be $\sim$0.4–0.6 nN. The scans consist of 256 lines with 256 data points each.

The mechanical properties of the cells were measured by acquiring force curves with the AFM (Schneider et al., 2000). In this mode, the probe is placed at a specific position in the P, C domain, and T zone, respectively, with the *xy* scan axes being disabled. The force applied to the probe is sensed through the deflection of the cantilever as the probe is approached to the growth cone and indented into the growth cone with the piezo. The applied force is calculated using Hooke's law and is proportional to the stiffness of the cantilever and the cantilever displacement. The indentation depth is calculated from the difference of the piezo displacement between IP (initial point of contact of the tip with the sample) and PD (range of piezo displacement at imaging force of 0.4–0.6 nN) as shown in Figure 4A. For example, an indentation depth of 160 nm was determined in the P domain at 0.5 nN imaging force. In this measurement we have neglected the deflection of the cantilever due to the very low elastic modulus of the growth cones. The various indentation depths at the typical imaging force of 0.5 nN were added to the measured heights to determine the actual average heights of P and C domain as well as of the T zone (see Fig. 4 and Table 1).

Data Analysis

AFM height images, cross sections, and volume data were prepared with IGOR Pro 5 software (WaveMetrics, Portland, OR). The raw data was filtered with a line flattening filter normalized to the glass surface to minimize the influence of 1/*f* noise, and the glass surface level was set to zero using a plane fit filter to directly compare different growth cones samples. Average heights plus standard deviations of the different growth cone regions were determined from a total of six growth cones with at least 1–4 different scans per growth cone (Table 1). Volumes were calculated by identifying specific regions of the image using the threshold function and summing the height of the voxels in the selected region. Fluorescence intensity scan lines of dextran-injected cells were obtained with the line scan tool in Metamorph 6.2 at the same locations as the AFM scans were set. To identify the same scan line positions, AFM and fluorescent images were overlaid and adjusted as accurately as possible with Photoshop 7.0 software (Adobe Systems, San Jose, CA). The accuracy of the mapping of the AFM image onto the fluorescence image was limited to about 100 nm, which was determined by the resolution of digitized optical microscopy images. Relative fluorescence intensity data and AFM height data were presented in terms of an integer proportional to the total measured light intensity and height, respectively.

RESULTS

Morphology of *Aplysia* Bag Cell Neuronal Growth Cones Visualized by Optical Microscopy

Aplysia bag cell neurons elaborate large growth cones when cultured on poly-L-lysine-coated glass coverslips (Fig. 1). The low magnification phase contrast

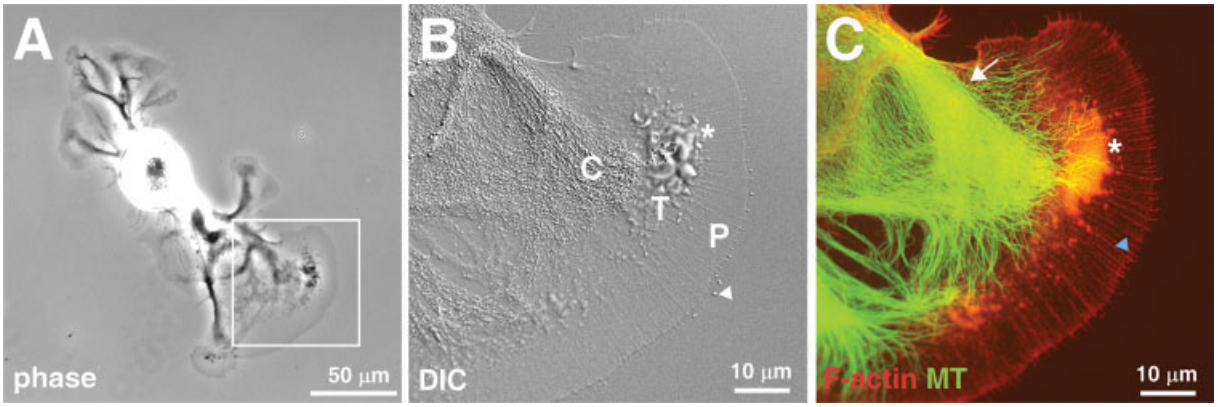

Figure 1 *Aplysia* growth cones visualized with optical microscopy. (A) Low magnification phase contrast image of a live bag cell neuron cultured on polylysine coated glass coverslips for 1 day. The largest growth cone is marked by a white box and shown at higher magnification in (B). (B) High magnification DIC image of the live growth cone marked in (A). Central (C) and peripheral (P) domain as well as transition (T) zone are indicated. The arrowhead points towards an enlarged filopodial tip. The T zone contains ruffling activity (marked with a white asterisk) that is rich in F-actin (see panel C). (C) Phalloidin labeling of F-actin (red) and microtubule immunocytochemistry (green) after fixation. Several different F-actin structures occur in the growth cone, including filopodial bundles (blue arrowhead), ruffles in the T-zone (white asterisk), and transverse F-actin arcs in the T-zone (white arrow). Microtubules are mainly located in the C domain, while highly dynamic microtubules explore the P domain (Schaefer et al., 2002; Suter et al., 2004). Scale bars as indicated.

image in Figure 1(A) shows a live bag cell neuron after 1 day in culture, with four major processes emerging from the neuronal cell body. At this stage in culture, *Aplysia* neuronal growth cones can exhibit diameters of 50–200 μm, being 5–10 times larger than their vertebrate counterparts. The large growth cone in the boxed area in the lower right of Figure 1(A) is shown at higher magnification in Figure 1(B) using DIC microscopy. Three major cytoplasmic growth cone domains can be clearly distinguished [Fig. 1(B)]: the central (C) and peripheral (P) domains are separated by the transition (T) zone. The C domain contains a high density of large DIC-refractive organelles that are transported both anterogradely and retrogradely on microtubule tracks [Fig. 1(B,C)]. In DIC optics, the presence of these large organelles makes it relatively easy to discern the C domain boundary with the next region, the T zone [Fig. 1(B)]. This zone is mainly characterized by the dynamic and random movement of ruffles or intrapodia (Rochlin et al., 1999), which are driven by *de novo* F-actin assembly [asterisk in Fig. 1(B,C)]. These dynamic F-actin-rich ruffles are always concentrated in the direction of growth cone advance, while C domain microtubules are focused towards them [Fig. 1(C)]. Changing the *z*-focus during DIC time-lapse imaging reveals that these ruffles are of significant height; they can also be discerned as phase-dark structures using low magnification phase contrast imaging [Fig. 1(A)]. The most distal cytoplasmic growth cone domain is the P domain, which is typically a 10–20 μm wide band that appears as a very thin region with alternating lamellipodia and filopodia [Fig. 1(B)]. The P domain features with the highest contrast are equally spaced filopodia spanning the P domain and extending past the perpendicular leading edge. These filopodia are a hallmark of growth cone cytoskeletal organization, consisting of bundles of actin filaments with their plus ends oriented towards the tips (Letourneau, 1983; Lewis and Bridgman, 1992; Schaefer et al., 2002). After 1–2 days in culture on poly-L-lysine substrate, filopodia of these young growth cones are typically short (1–3 μm long), frequently carrying an enlarged tip [white arrowhead in Fig. 1(B)].

To visualize the distribution of the major two cytoskeletal structures, microtubules and F-actin, growth cones were chemically fixed and processed for fluorescent labeling [Fig. 1(C)]. Microtubules are detected predominantly in the C domain, while a few microtubules penetrate into the P domain at any given time. These are highly dynamic microtubules that use the filopodial F-actin bundles as polymerization guides to explore the P domain (Schaefer et al., 2002; Suter et al., 2004). F-actin staining with Alexa 568-phalloidin reveals four major F-actin organizations in

the P domain and T zone: (1) filopodia bundles [blue arrowhead in Fig. 1(C)]; (2) less organized actin filament meshwork between filopodia; (3) ruffles or intrapodia [asterisk in Fig. 1(C)]; and (4) transverse actin arcs [white arrow in Fig. 1(C)]. These F-actin structures in neuronal growth cones have been described in detail (Forscher and Smith, 1988; Lewis and Bridgman, 1992; Rochlin et al., 1999; Schaefer et al., 2002).

AFM Imaging Reveals Significant Height Differences Between Cytoplasmic Growth Cone Domains

Fixed *Aplysia* bag cell growth cones were imaged with both DIC optical microscopy and AFM. We chemically fixed the cells in the present study, since higher resolution AFM images can be acquired when compared to live cells (Braet et al., 1998). First, suitable cells elaborating large, well-structured growth cones were selected [Fig. 2(A)]. Next, the growth cones [boxed area in Fig. 2(A)] were visualized with a 60× high resolution DIC objective right before [Fig. 2(B)] and after chemical fixation [Fig. 2(C)]. Note the extensive ruffling activity in the T zone as seen in the live cell image [asterisk in Fig. 2(B)]. After fixation, the contrast in this ruffling region appeared decreased in the DIC images when compared to the live condition [Fig. 2(B,C)]. A general flattening of the T zone could also be observed, while the heights of the P and C domain and axonal shaft did not appear to have changed after fixation as judged by DIC visualization. Thus, overall growth cone features were very well preserved by the fixation procedure.

AFM images of the growth cones were acquired in the constant force imaging mode, in which the probe was rastered over the cell surface at a constant cantilever deflection using an optimized feedback control loop. Imaging forces of 0.4–0.6 nN were found to be the lowest forces that could be practically used to maintain clear imaging while minimizing damage to the cells. The boxed growth cone area of Figure 2(B,C) is shown as an AFM height image in Figure 2(D). The structure of the growth cone imaged by the AFM is depicted with gray-scale encoded height information in this figure. The subcellular regions including filopodia, lamellipodia, ruffling region, and C domain can be clearly identified in this AFM image. Cross sections through the growth cone along the fast scanning axis [Fig. 2(D,E)], indicated that the P domain lamellipodia are very flat and fairly uniform throughout the growth cone with the heights varying between 40 and 50 nm when measured against the substrate surface. The green and blue horizontal cross sections in Figure 2(E) show that the ruffling region of this fixed growth cone is almost as tall as the C domain. The highest point of the ruffling region is about 600 nm above the substrate, while the C domain is only slightly higher. Both the T zone and the C domain height profiles are not smooth, but exhibit consecutive small elevations in the range of 20–100 nm. A three-dimensional reconstruction of this growth cone is shown in Figure 2(F). Besides revealing the elevated transition zone ruffles and the C domain, the reconstruction also shows that the tips of filopodia and certain structures in the P domain are thicker than surrounding areas (both features are shown at higher resolution in Fig. 3).

Another growth cone AFM image is shown in Figure 2(G). This growth cone exhibited less extensive T zone ruffling activity with heights around 300 nm [green vertical cross section in Fig. 2(G,H)] when compared with the example shown in Figure 2(D,E). The violet scan line cuts through the C domain reaching a top height of 800 nm [Fig. 2(G,H)]. Furthermore, the AFM image clearly resolved linear structures reminiscent of filopodial F-actin bundles crossing the P domain [Fig. 2(G)]. These structures are taller than the intermittent P domain lamellipodia, which is composed of an actin filament meshwork. High resolution scans revealed a 20 nm height difference between the filopodial bundles and the adjacent peripheral lamellipodia [Fig. 3(C,D)].

The average heights of the different growth cone regions were determined for six growth cones (Table 1). The P domain is fairly uniform, exhibiting an average height of 53 ± 24 nm (mean ± standard deviation). The filopodia are 73 ± 11 nm high in the P domain and 38 ± 14 nm high when emerging from the leading edge. The increased heights of the P domain filopodia versus the average P domain are likely due to the high density of actin filaments in the filopodia. The T zone average height is 577 ± 175 nm. The increased standard deviation of the T zone height is attributed to the presence of variable ruffling in this region. The C domain exhibits an average height of 1020 ± 191 nm. It is important to note that heights of 160 nm for the P domain, 220 nm for the ruffling T zone, and 200 nm for the C domain have to be added to the figures presented in Table 1 (last column), in order to compensate for the specimen indentation occurring at an imaging force of 0.5 nN, therefore resulting in height values that are closer to real heights (see section on mechanical properties, Fig. 4 and discussion). In summary, AFM data generally match the structural features derived from DIC

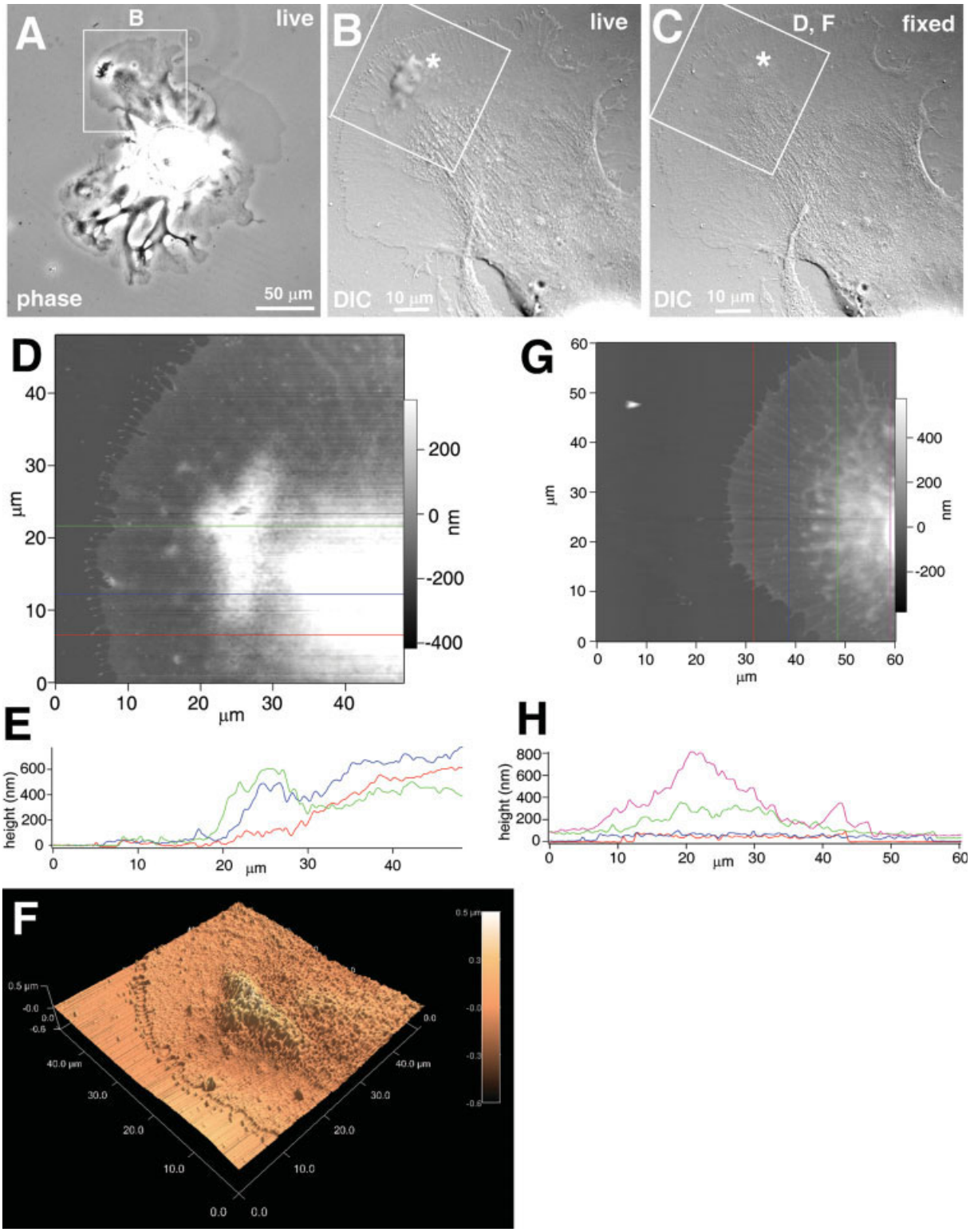
A
B
live
phase
50 µm
B
live
DIC
10 µm
C
D, F
fixed
DIC
10 µm
D
µm
nm
200
0
-200
-400
G
µm
nm
400
200
0
-200
E
height (nm)
µm
H
height (nm)
µm
F
0.5 µm
40.0 µm
30.0
20.0
10.0
0.0

Table 1 Average Heights of Different Growth Cone Domains

Domain	Average Height (nm)	Standard Deviation (nm)	SEM (nm)	*n*	Average Corrected Height (nm)
P domain	53	24	3	82	213
P domain filopodia	73	11	2	24	–
Filopodia shafts	38	14	3	29	–
Filopodia tips	96	35	7	23	–
T zone ruffles	577	175	50	12	797
C domain	1,020	191	61	10	1,220

For each growth cone 1–4 different AFM images were acquired. For each image, 5–12 random line scans were selected to determine the average height in a particular growth cone region. *n* is the number of measurements taken for that particular domain in six different growth cones. Heights were determined in contact imaging mode with the AFM operating at a constant force of 0.4–0.6 nN. To account for deformation at this force, 160 nm have to be added to the P domain heights, while 220 and 200 nm have to be added to the heights of the T zone ruffles and C domain, respectively (last column).

images; however, the height measurements clearly reveal that the differences between T zone/C domain and the P domain are significantly larger than the DIC images suggest.

High Resolution AFM Images of the Leading Edge of the Growth Cone

Filopodia are fingerlike structures that continuously extend and retract from the leading edge of the growth cone with important functions for the detection of guidance cues as well as signaling and motor functions during growth cone steering (Kater and Rehder, 1995; Jay, 2000; Gallo and Letourneau, 2004). To examine the P domain filopodia and lamellipodia in more detail, these growth cone regions were imaged at higher resolution with the AFM (see Fig. 3). The leading edges of two different growth cones with several filopodia emerging are shown in Figure 3(A,C). The filopodia tips shown in Figure 3(A) are significantly enlarged when visualized with the AFM. Such enlarged filopodia tips can also be observed by DIC optics [Fig. 1(B)] in live growth cones and have previously been reported as well (Wu and Goldberg, 1993; Lin et al., 1996; Suter and Forscher, 2001). Thus, the enlarged tips are clearly not an artifact induced by the chemical fixation. The tip enlargement was found to be associated preferentially with short filopodia in young growth cones slowly advancing on polylysine substrate, while longer filopodia without enlarged tips are associated with growth cones advancing on growth promoting substrates (Wu and Goldberg, 1993).

The dimensions of the enlarged filopodia tips have been characterized in more detail. Cross sections through the tips and shafts of filopodia as well as along the length of a single filopodium revealed that the tips are in average three times higher than the shafts [Fig. 3(A,B); Table 1]. The filopodia shafts have an average height of 38 ± 14 nm (mean ± SD, $n = 29$) and are 200–250 nm wide. The heights of the filopodia tips in the growth cone shown in Figure 3(A) are between 120 and 140 nm, with correspond-

Figure 2 AFM imaging reveals significant height differences in various growth cone regions. (A) Low magnification phase contrast image of a live bag cell neuron. (B) High magnification DIC image of the live growth cone shown in the boxed area in (A). (C) DIC image of the same growth cone right after fixation. The structural details of the growth cone are well preserved after fixation; however, the height of the ruffling activity in the T zone (indicated by white asterisk) appears reduced after fixation when compared to the live image shown in (B). The boxed area reflects the AFM scanning area shown in (D). (D) AFM height image of the growth cone region marked with a white box in (B) and (C). (E) Color-coded plots of height distributions resulting from the horizontal scan lines indicated in (D). Average P domain heights were around 50 nm in the growth cone shown, while average T zone ruffling heights were an order of magnitude higher (500 nm). The highest growth cone region was detected in the C domain (around 700 nm). (F) Three-dimensional reconstruction of growth cone shown in (D). Tips of filopodia are elevated when compared to the filopodia shafts. Height information in *z*-axis is color-coded. (G) Height AFM image of a different growth cone including vertical scan lines. The filopodial F-actin bundles crossing the P domain have higher elevations than adjacent lamellipodial regions. This is also visualized by the wavy appearance of the red height profile in (H). The ruffling zone of this growth cone is not as high as the one shown in A–F. Dimensions are as indicated with scale bars (A–C) or on the axes of the AFM images.

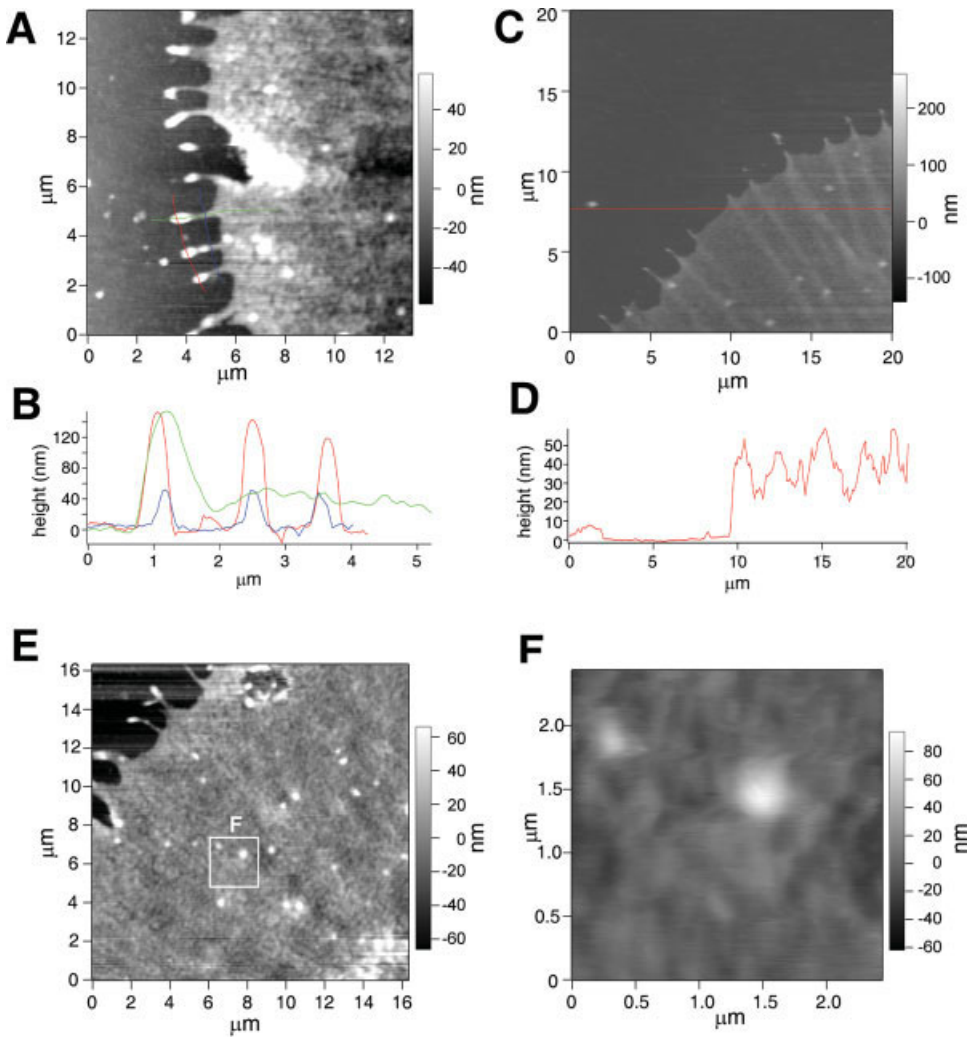

Figure 3 High resolution AFM scans show enlarged filopodia tips. (A) and (C) High resolution AFM height images of the leading edge regions of two different growth cones. (B) and (D) show the respective height profiles of the scan lines indicated. Scan lines in (B) reveal that the filopodia tips are significantly higher and wider than their shafts. Red scan line in (C) and (D) demonstrates that the heights of P domain filopodial bundles are about 20 nm higher than adjacent lamellipodial areas. (E) High resolution height image of another P domain example which shows the topography in more detail. (F) Boxed area in (E) is further magnified to reveal round elevated area of 80–100 nm height. Dimensions are as indicated.

ing widths of 300–400 nm. The average height of filopodia tips is 96 ± 35 (mean ± SD, $n = 23$; Table 1). Volume measurements (see Methods) revealed that the volumes of the enlarged tips varied between 0.02 and 0.04 μm^3 ($n = 12$).

In several growth cones we were able to clearly image structures reflecting the filopodial F-actin bundles crossing the P domain [Fig. 3(C,D)]. These filopodia are 20 nm higher than the average P domain areas with a height of 73 ± 11 nm (mean ± SD, $n =$ 24; Table 1). Besides these radial bundles that make up the filopodia, the P domain apparently does not exhibit much variation in height. However, we could observe some additional fine structural details in high resolution scans [Fig. 3(E,F) also visible as white dots in Fig. 3(A,C)]. These round areas have a diameter of 0.3–0.5 μm diameter, with heights of 80–100 nm. We do not know what these focal elevations visualized by AFM are. They could represent either special growth cone features or small particles on the substrate. The density of these features in the P domain is clearly higher than on the polylysine areas that

have not been contacted by the growth cone, an observation which is in support of the former explanation [Fig. 3(C)].

Mechanical Properties of the Growth Cone

Mechanical measurements were made at different loading forces to determine the influence of the microscope's imaging force on the measured volume and the stiffness of the different growth cone regions. The cantilever deflection-piezo displacement curves shown in Figure 4 were recorded at specific locations on either the P, C domain, or the T zone of the growth cone. Since force is directly proportional to cantilever displacement, these curves represent the force the AFM probe experiences as it approaches the surface of the growth cone and then indents into the sample (see Methods for further explanation of force-curve analysis). Figure 4(A) illustrates a series of five force-versus-piezo displacement curves that were made on the P domain lamellipodia at increasing maximum forces. Three trends can be observed in these force curves. First, the cantilever deflection [Fig. 4(A), right axis) increased slowly as the probe was pressed into the surface of the lamellipodia, which is an indication that this region of the growth cone was very soft. In fact, at an imaging force of 0.5 nN the probe indented $\sim$160 nm into the surface of the P domain, i.e., the probe contacts the surface at the piezo position marked with IP and images the surface in the piezo region marked with PD. This is an important observation as it indicates that the AFM contact mode images taken at 0.5 nN do not reflect the real height of the P domain. The second observation was that the form of the indentation curves is dependent on the maximum force applied to the P domain. That is, the slope of the force-versus-displacement curve increased as the maximum force applied to the P domain increased. Third, there was hysteresis

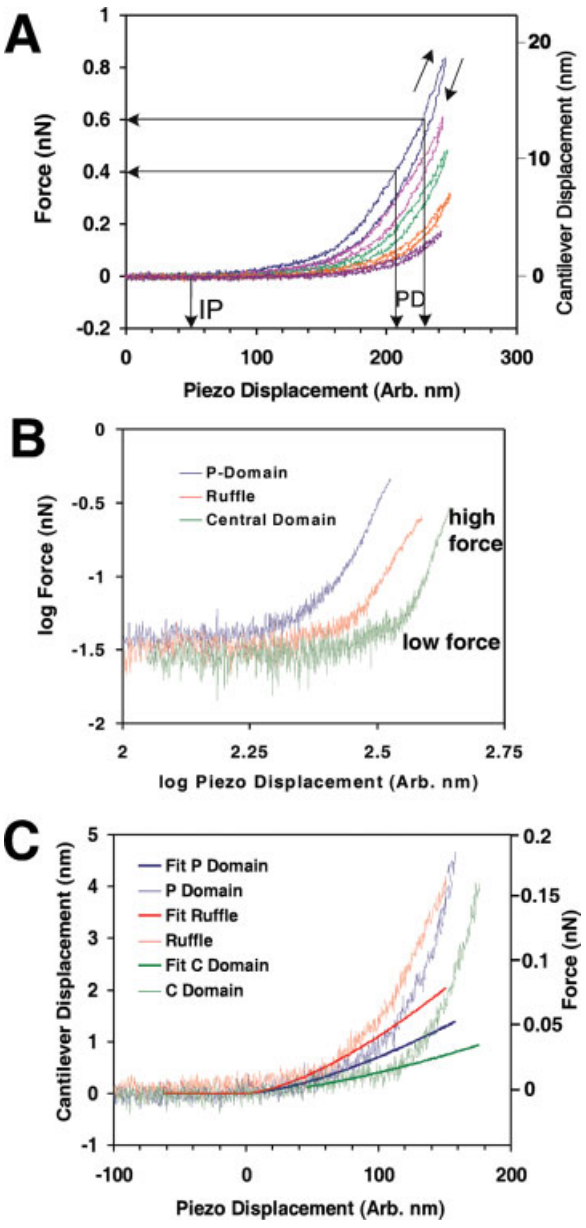

Figure 4 Force curve analysis to determine mechanical properties. (A) A series of five cantilever displacement (or force) versus piezo displacement curves that were made on the P domain lamellipodia at increasing maximum forces and plotted on a linear scale. These curves have been prepared so that positive forces are associated with indentation of the probe into the growth cone and the piezo displacement axes are offset to align the maximum force at $\sim$250 nm. IP identified the initial point of contact of the probe with the surface of the cell in the highest load force curve (blue curve). PD is the range of piezo displacements during imaging of the P domain at a force between 0.4 and 0.6 nN. Thus, the indentation depth is the difference of the piezo displacement between IP and PD and was determined as 160 nm in the P domain at 0.5 nN. Upwards arrow indicates increasing force, downward arrow indicates decreasing force. (B) Representative force curves from the P domain, ruffling region, and C domain which are presented as log force-versus-log piezo displacement. The log–log scale has been used to highlight the change in the mechanical properties of the cell as a function of load. At low force loads the curves reveal soft homogenous material; at higher force loads the curves reveal harder material (cytoskeleton). (C) Low loading force curves on a linear scale from the three regions of a different growth cone and the fit of the Hertzian contact equation to this data. The reduced Young's modulus of the P domain, ruffling region, and C domain were determined from these fits (see Results).

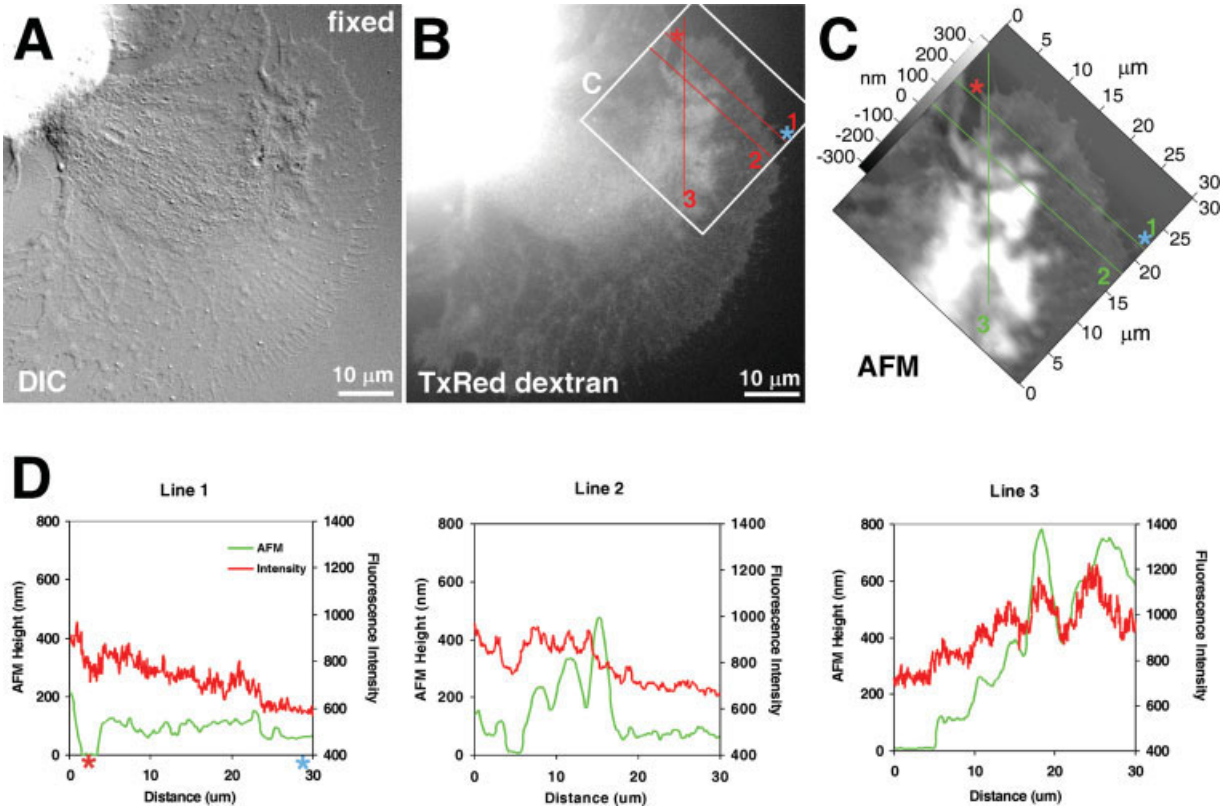

Figure 5 Comparison of fluorescence volume and AFM imaging. (A) DIC image of fixed bag cell growth cone 1 h after injection with lysine fixable 3 kDa Texas Red dextran. The ruffling region as well as other details of the growth cone have been well preserved during the chemical fixation process. (B) Fluorescence image of Texas Red dextran of the same growth cone reveals an intensity distribution that corresponds to volume. The boxed area shows the region used for the AFM scan in (C) plus three scan lines (red) used to directly compare fluorescence intensity and AFM height data. The coverslip positions of scan line 1 are indicated with a red and blue asterisk in (B), (C), and (D). (C) AFM height image of the boxed area of interest. (D) The three line scans indicated in (B) and (C) were plotted as AFM height data (green line) and relative fluorescence intensity of Texas Red dextran (red line). Dimensions as indicated by scale bars.

in the advancing and retracing force curves, which is indicative of plastic deformation of the P domain induced by the sharp AFM probe.

Representative force curves measured in the P domain, ruffling region and C domain are presented in Figure 4(B). The force data is presented on a log force-versus-log piezo displacement scale to highlight the similarity in the mechanical response of the different regions of the cell and the change in the mechanical properties of the cell as a function of load. At loads (F) below about 0.1 nN, the deformation (δ) of all three regions of the growth cone can be seen to follow the power law of the form $F \propto \delta^n$, where $n =$ 1.5. This type of behavior is characteristic of the deformation of soft homogenous materials, such as plasmamembrane, described by Hertzian contact mechanics. At higher loads all three regions of the growth cone appear to be deformed much more slowly, i.e., the scaling parameter n increases to a value between 6 and 9. At force loads above 0.1 nN, the AFM probe reveals harder material such as cytoskeletal structures [F-actin bundles in Fig. 3(C)].

The stiffness of the different growth cone regions can be determined for the low load force curves using contact mechanics (Dimitriadis et al., 2002). The equation for the indentation of a spherical indenter into a homogenous material was first derived by Hertz (Hertz, 1881):

$$F = \frac{4E^* R^{1/2}}{3} \delta^{3/2}$$

where E^* is the reduced Young's modulus, R is the radius of curvature of the spherical indenter, and δ is the indentation depth. Figure 4(C) shows a fit of this equation to the force curves acquired in the different

regions of a growth cone revealing that the fit matches the experimental data only in the very low force regime. The reduced Young's modulus of the P domain, ruffling region, and C domain were determined as 110, 200, and 70 kPa, respectively. Thus, the C domain was determined as the softest region in the growth cone, while the ruffling region and the P domain are stiffer.

AFM and Optical Volume Profiles Provide Similar Results

Fluorescently labeled probes are frequently used in cell biology to determine the relative volume of specific subcellular regions to normalize the fluorescence intensity signal of a protein of interest against the volume of the cell. Dextran is an inert carbohydrate molecule that is available in various sizes and is commonly used as a volume marker as well as a tool to determine the accessibility of intracellular compartments. We have directly compared the relative volumes of specific regions of the cell as determined by lysine-fixable Texas Red-labeled dextran (3 kDa) with AFM images taken from the same growth cones. Bag cell neurons were allowed to recover for 1 h in the dark after injection with Texas Red dextran before fixation. Then fluorescent images were captured, followed by AFM imaging.

DIC images taken right after fixation of the cells [Fig. 5(A)] show structural information that qualitatively corresponds well with the fluorescent volume [Fig. 5(B)] and AFM images [Fig. 5(C)], respectively. The fluorescent dextran and AFM images revealed similar trends with respect to the volumes of specific growth cone regions. They both show that the P domain is relatively flat, while the ruffling region in the T zone as well as the C domain are significantly higher. Comparison of the fluorescence intensity of specific features with heights measured with the AFM in the ruffling region suggests a linear relationship between fluorescence intensity and height, with $\sim$0.5 fluorescence intensity units equivalent to 1 nm of measured height [Fig. 5(D)]. However, line scan analysis and direct comparison of the data achieved by the two methods revealed some interesting differences. The data from three line scans taken at the same locations of the growth cone shown in Figure 5(B,C) are plotted in Figure 5(D). The main difference in these two methods results from the lateral resolution of the techniques. Highly intense fluorescence regions such as the cell body caused out of focus fluorescent glare that increased signals in adjacent areas when imaged with a conventional fluorescence light microscope. This adds a gradient of intensity values that do not reflect actual height information; e.g., compare fluorescence intensity and AFM height plot of scan line 1 in Figure 5(D). The red and blue asterisks indicate the coverslip position of scan line 1. At the red asterisk, which is closer to the cell body, there is a larger background fluorescence intensity level than at the blue mark (closer to the leading edge of the growth cone). Thus, areas of high fluorescent intensity can cause a gradient of fluorescent signals, making adjacent areas appear taller than they actually are when compared with substrate areas further away from the cell body. When a line scan (3) was performed vertically on the growth cone in Figure 5, we did not observe the additional gradient induced by the cell body fluorescence, and the two scan profiles were matching significantly better than in the case of scan lines 1 and 2. Finally, fluorescent volume markers imaged with widefield epifluorescence suffer in both resolution and signal to noise ratio when compared to AFM imaging. The direct comparison of the scan line data revealed that a 40–50 nm height difference (as determined by AFM) can still be detected by the fluorescent volume marker. The AFM on the other hand has a z resolution in the range of 1–5 nm in case of our growth cone measurements and provides much greater detail at a better signal to noise ratio. In summary, our findings reveal that fluorescence imaging is a suitable method to get information on the relative volume distribution in the growth cone. However, AFM imaging results in quantitative volume data at higher resolution.

DISCUSSION

Our study resulted in the following key findings: (1) we have provided the first detailed quantification of the three-dimensional morphology of neuronal growth cones. (2) Our direct comparison of optical and AFM imaging of the same growth cones revealed that DIC and fluorescence techniques provide a qualitative estimate of cell volume information, while AFM data give us quantitative height information of specific growth cone regions at much greater resolution and better signal to noise ratio. (3) Force analysis revealed that growth cones contain soft material with distinct stiffness in different growth cone domains, and harder material (cytoskeleton) that can be clearly revealed by AFM imaging. (4) Some filopodia tips have volumes that are 4–5 times larger than their shafts. The quantitative and qualitative findings of our current study will contribute to a better understanding

of the biophysical and biochemical processes underlying neuronal growth cone motility and guidance.

AFM and Optical Imaging of Neuronal Growth Cones

We have used *Aplysia* bag cell neurons for our studies because they elaborate large, relatively flat growth cones on polylysine substrate. Since higher resolution can be achieved with fixed samples compared to live cells (Braet et al., 1998), we chemically fixed the growth cones. Direct comparison of live and fixed growth cones with DIC optics [Fig. 2(B,C)] indicates that the growth cones were well preserved with our fixation protocol, although a certain flattening effect can be observed, particularly in the T zone [asterisk in Fig. 2(B,C)]. However, one has to be careful with the interpretation of DIC images. While they provide good information about cell morphology, height information is not quantitative, since the plain polarized light can be affected both by the amount and nature of the material it passes through. While the DIC images suggest a flattening of the T zone ruffling after fixation, AFM height data reveal a 10-fold height difference between the lamellipodia and the ruffling region (see Fig. 2). The direct comparison of fluorescent volume and AFM data (see Fig. 5) indicate that the two methods are generally in good agreement, however, AFM data are of higher resolution and do not suffer from out of focus glare.

In interpreting the height images, it is important to take the applied force as well as the mechanical properties of the cell into account. At low force loads ($<$0.1 nN), the mechanical properties of the growth cone were measured using force curves and interpreted with Hertzian contact mechanics [Fig. 4(C)]. The reduced elastic modulus of the P domain, T zone ruffles, and C domain were in the ranges of 85–135, 176–225, and 45–95 kPa, respectively. These values of moduli are consistent with previous measurements on fixed cells and about two orders of magnitude higher than the values that are typically measured on living cells (Braet et al., 1998). At low loads ($<$0.1 nN), the cell responds slowly to the applied force, which is characteristic of soft homogeneous materials. Indentation curves at loads greater that 0.1 nN revealed a different mechanical behavior that is highlighted by the abrupt increase in slope of the log (force)-versus-log (piezo displacement) curves presented in Figure 4(B): the cell responds quickly to the applied force, which is an indication of a harder substrate (most likely F-actin cytoskeleton). It has been previously shown that cell stiffness increases with the polymerization state of the actin cytoskeleton (Wakatsuki et al., 2001). The actual heights of distinct growth cone regions have been determined by measuring the indentation at the typical imaging force of 0.5 nN, derived from the advancing force curves as shown in Figure 4(A). Adding these indentation values (160, 220, and 200 nm for P domain, T zone ruffles, and C domain, respectively) to the measured heights resulted in the real heights shown in the last column of Table 1.

Although the AFM and the cytoskeletal fluorescence images were not acquired simultaneously, it is clear that the constant force AFM images are dominated by F-actin structures in the P domain and microtubules in the C domain. Microtubules and F-actin bundles have bending stiffness in the order of 1 GPa (Gittes et al., 1993), thus four orders of magnitude higher than that of the crosslinked cytoplasmic material of P domain. A structure with a reduced Young's modulus of 1 GPa will deform only 0.2 nm when indented by a spherical indenter of 20 nm radius (size of the tip used in our study) at a load of 0.5 nN. This explains why the F-actin bundles crossing the P domain are clearly visible in Figures 2(D,F) and 3(C). Furthermore, this conclusion is consistent with previous measurements of living endothelial cells in which actin bundles were the only cellular elements resolved by contact mode AFM (Pesen and Hoh, 2005).

We are aware that the heights of certain growth cone regions as well as the determinations of elastic moduli are affected by the chemical fixation protocol. Particularly, in the transition zone we have observed ruffles and spine-like structures in live growth cones that appear higher than 1 μm when imaged with DIC optics (data not shown). Such elevated dynamic protrusions termed intrapodia emerging from the T zone have also been reported in vertebrate growth cones (Rochlin et al., 1999; McNally and Borgens, 2004). Future studies will focus on determining the heights and elastic moduli of these structures as well as all other growth cone regions with AFM imaging under live cell condition. Will we be able to reveal the topography and structural features of live growth cones at a similar level of resolution as in the present study? The primary limitations are the dynamics of the growth cone and the scanning speed of the instrument, which is currently 20 min for a 50 μm by 50 μm field. We are aware that many cytoskeletal-driven dynamic processes in the growth cone occur at speeds of 0.1–10 μm/min, thus further instrument development or reducing the scanning area will be required to fully take advantage of the resolution of the AFM for live growth cone analysis. We expect that the elastic moduli of the different growth cone regions will be in the range of 1 kPa for living cells based on previous work (Rotsch et al.,

1997; Pesen and Hoh, 2005). It will be very interesting to determine the total stiffness of the distinct regions in live growth cones and to investigate a potential correlation with the stiffness of the substrate the growth cone is interacting with; particularly in light of previous studies revealing that cells can adapt receptor-cytoskeletal linkage strength to extracellular matrix rigidity (Choquet et al., 1997).

Although a few studies have used the AFM to image neuronal structures (Parpura et al., 1993; Bonfiglio et al., 1995; Lal et al., 1995; Tojima et al., 2000; McNally and Borgens, 2004; Ricci et al., 2004; McNally et al., 2005), only four reported on growth cones (Lal et al., 1995; McNally and Borgens, 2004; Ricci et al., 2004; McNally et al., 2005). These studies provided only limited information on the heights of distinct growth cone regions, largely because the neuronal cells selected did not elaborate large, well developed growth cones or because the imaging data were acquired with deflection or other poorly defined modes. In deflection mode, in which the deflection of the cantilever is sensed with the feedback loop partially disabled, local differences in height are accentuated, but the height does not reflect a well defined parameter. The exception in these studies was Ricci et al. 2004, who measured both lamellipodia and filopodia heights in chick embryonic spinal cord growth cones in a pseudo-constant force mode. Interestingly, although completely different types of neurons used, the height data for the lamellipodia are quite similar when comparing our data (213 nm corrected height) with Ricci et al., 2004 (30–60 nm for live and 100–200 nm for fixed growth cones). Other studies reported a range of growth cone heights not determined in specific regions, e.g., 50–700 nm for live PC-12 cells (Lal et al., 1995), or an average growth cone height of 260 nm for live chick DRG neurons (McNally and Borgens, 2004; McNally et al., 2005). In summary, our data on *Aplysia* growth cones are in general agreement with previously published work providing less detailed height information in vertebrate growth cones. Finally, our data are consistent with cross sectional measurements taken from electron microscopy images of developing or regenerating growth cones *in vivo* (Scalia and Matsumoto, 1985; Williams et al., 1991; Xue and Honig, 1999).

High Resolution Imaging of Filopodia Tips

It has been previously reported that filopodia tips in *Aplysia* growth cones cultured on polylysine can be enlarged when observed in live cells with DIC microscopy (Wu and Goldberg, 1993; Lin et al., 1996; Suter and Forscher, 2001). These findings have been confirmed in the present study [Fig. 1(B)]. Thus, the enlarged tips measured by high resolution AFM imaging are not an experimental artifact. The enlarged tips correlate well with the high concentration of tyrosine-phosphorylated proteins detected by at the endings of filopodia, although increased phosphotyrosine levels can also be found in tips that are not enlarged (Wu and Goldberg, 1993; Suter and Forscher, 2001). These proteins are believed to be involved in the signal transduction downstream of cell surface receptors, receptor localization, as well as in the regulation of actin-dependent filopodia dynamics (Goldberg and Wu, 1996). Which specific proteins have been identified in filopodia tips so far? Immunolocalization revealed an enrichment of β_1-integrin and active Src family tyrosine kinase at the tips of *Aplysia* growth cone filopodia (Wu et al., 1996; Suter and Forscher, 2001). In vertebrate growth cones, the following proteins were detected in high concentration at filopodia tips: ERM proteins (Wu et al., 1996), mena (Lanier et al., 1999), active Src, Cdc42, and PAK (Robles et al., 2005), WAVE proteins (Nozumi et al., 2003), and myosin-X (Berg and Cheney, 2002). Thus, the larger volume observed in the enlarged tips compared to the filopodia shafts are likely due to a high concentration of proteins important for signaling downstream of guidance cues and for regulation of filopodial F-actin dynamics. This high local protein concentration may result in volume increase because of swelling; however, asymmetric membrane protein and lipid composition at the filopodia tips could also contribute to the enlarged tips.

CONCLUSION

Quantitative information on the morphology and dimensions of distinct growth cone regions are important to understand how proteins and other molecules can move from one growth cone compartment to another either by passive diffusion, active motor driven transport, or cytoplasmic flow. The AFM promises to provide this quantitative information in the growth cone, particularly in future live cell studies. An improved knowledge of protein translocation will be relevant for a better mechanistic understanding of several processes in the growth cone, including distribution and activation of signaling enzymes, signal transduction between the cell membrane and the underlying cytoskeleton, and turnover of cytoskeletal polymers and distribution of subunits. How can we compare *Aplysia* growth cones with cones from other species? It will be difficult to achieve a similar level

of resolution and information with AFM imaging of vertebrate growth cone because they are smaller and more dynamic than *Aplysia* growth cones. However, comparison of our height measurements with published data on vertebrate growth cone thickness revealed that heights are similar between vertebrates and invertebrates, while *Aplysia* growth cones exhibit significantly larger *xy* dimensions *in vitro*. In the case of the *Aplysia* growth cone, the distance from the leading edge to the central domain for example is about 100 times larger than the height in the P domain (about 30 times in the case of vertebrate growth cones). Thus, in both *Aplysia* and vertebrate growth cones, protein translocation by passive diffusion from the plasma membrane at the leading edge towards the P domain F-actin cytoskeleton takes significantly less time than towards the C domain microtubule cytoskeleton. To compensate for these differences, the flat morphology plus the retrograde F-actin flow allow the growth cone to channel proteins more efficiently towards microtubules that are further away from the leading edge than the actin cytoskeleton. For experimental reasons most growth cone studies are carried out *in vitro*, where all growth cones exhibit a relatively flat morphology. Although *in vivo* growth cones have various shapes and sizes depending on their location and speed of growth; large lamellipodia-rich growth cones have been also found *in vivo* (Scalia and Matsumoto, 1985; Williams et al., 1991; Xue and Honig, 1999; Mason and Erskine, 2000). Thus, *in vitro* studies can provide important insights into growth cone biology that may likely hold true *in vivo*.

The authors thank Dr. Peter Hollenbeck for his comments on the manuscript and Mrs. Virginia Livingston for assistance in editing.

REFERENCES

Berg JS, Cheney RE. 2002. Myosin-X is an unconventional myosin that undergoes intrafilopodial motility. Nat Cell Biol 4:246–250.

Binnig G, Quate CF, Gerber C. 1986. Atomic force microscope. Phys Rev Lett 56:930–933.

Bonfiglio A, Parodi MT, Tonini GP. 1995. Subcellular details of early events of differentiation induced by retinoic acid in human neuroblastoma cells detected by atomic force microscope. Exp Cell Res 216:73–79.

Braet F, de Zanger R, Seynaeve C, Baekeland M, Wisse E. 2001. A comparative atomic force microscopy study on living skin fibroblasts and liver endothelial cells. J Electron Microsc (Tokyo) 50:283–290.

Braet F, Rotsch C, Wisse E, Radmacher M. 1998. Comparison of fixed and living liver endothelial cells by atomic force microscopy. Appl Phys Mater Sci Process 66: S575–S578.

Choquet D, Felsenfeld DP, Sheetz MP. 1997. Extracellular matrix rigidity causes strengthening of integrin-cytoskeleton linkages. Cell 88:39–48.

Dent EW, Gertler FB. 2003. Cytoskeletal dynamics and transport in growth cone motility and axon guidance. Neuron 40:209–227.

Dickson BJ. 2002. Molecular mechanisms of axon guidance. Science 298:1959–1964.

Dimitriadis EK, Horkay F, Maresca J, Kachar B, Chadwick RS. 2002. Determination of elastic moduli of thin layers of soft material using the atomic force microscope. Biophys J 82:2798–2810.

Dvorak JA. 2003. The application of atomic force microscopy to the study of living vertebrate cells in culture. Methods 29:86–96.

Engel A, Lyubchenko Y, Muller D. 1999. Atomic force microscopy: A powerful tool to observe biomolecules at work. Trends Cell Biol 9:77–80.

Forscher P, Smith SJ. 1988. Actions of cytochalasins on the organization of actin filaments and microtubules in a neuronal growth cone. J Cell Biol 107:1505–1516.

Gallo G, Letourneau PC. 2004. Regulation of growth cone actin filaments by guidance cues. J Neurobiol 58:92–102.

Gittes F, Mickey B, Nettleton J, Howard J. 1993. Flexural rigidity of microtubules and actin filaments measured from thermal fluctuations in shape. J Cell Biol 120:923–934.

Goldberg DJ, Burmeister DW. 1986. Stages in axon formation: Observations of growth of Aplysia axons in culture using video-enhanced contrast-differential interference contrast microscopy. J Cell Biol 103:1921–1931.

Goldberg DJ, Wu DY. 1996. Tyrosine phosphorylation and protrusive structures of the growth cone. Perspect Dev Neurobiol 4:183–192.

Green CP, Lioe H, Cleveland JP, Proksch R, Mulvaney P, Sader JE. 2004. Normal and torsional spring constants of atomic force microscope cantilevers. Rev Sci Instrum 75:1988–1996.

Henderson E, Haydon PG, Sakaguchi DS. 1992. Actin filament dynamics in living glial cells imaged by atomic force microscopy. Science 257:1944–1946.

Hertz H. 1881. Ueber die Beruehrung fester elastischer Koerper. J Reine Angew Math 92:156–171.

Huber AB, Kolodkin AL, Ginty DD, Cloutier JF. 2003. Signaling at the growth cone: Ligand-receptor complexes and the control of axon growth and guidance. Annu Rev Neurosci 26:509–563.

Jay DG. 2000. The clutch hypothesis revisited: Ascribing the roles of actin-associated proteins in filopodial protrusion in the nerve growth cone. J Neurobiol 44:114–125.

Kater SB, Rehder V. 1995. The sensory-motor role of growth cone filopodia. Curr Opin Neurobiol 5:68–74.

Lal R, Drake B, Blumberg D, Saner DR, Hansma PK, Feinstein SC. 1995. Imaging real-time neurite outgrowth and cytoskeletal reorganization with an atomic force microscope. Am J Physiol 269:C275–C285.

Lanier LM, Gates MA, Witke W, Menzies AS, Wehman AM, Macklis JD, Kwiatkowski D, Soriano P, Gertler FB. 1999. Mena is required for neurulation and commissure formation. Neuron 22:313–325.

Letourneau PC. 1983. Differences in the organization of actin in the growth cones compared with the neurites of cultured neurons from chick embryos. J Cell Biol 97:963–973.

Lewis AK, Bridgman PC. 1992. Nerve growth cone lamellipodia contain two populations of actin filaments that differ in organization and polarity. J Cell Biol 119:1219–1243.

Lin CH, Espreafico EM, Mooseker MS, Forscher P. 1996. Myosin drives retrograde F-actin flow in neuronal growth cones. Neuron 16:769–782.

Lin CH, Forscher P. 1993. Cytoskeletal remodeling during growth cone-target interactions. J Cell Biol 121:1369–1383.

Mason C, Erskine L. 2000. Growth cone form, behavior, and interactions in vivo: Retinal axon pathfinding as a model. J Neurobiol 44:260–270.

McNally HA, Borgens RB. 2004. Three-dimensional imaging of living and dying neurons with atomic force microscopy. J Neurocytol 33:251–258.

McNally HA, Rajwa B, Sturgis J, Robinson JP. 2005. Comparative three-dimensional imaging of living neurons with confocal and atomic force microscopy. J Neurosci Methods 142:177–184.

Nozumi M, Nakagawa H, Miki H, Takenawa T, Miyamoto S. 2003. Differential localization of WAVE isoforms in filopodia and lamellipodia of the neuronal growth cone. J Cell Sci 116:239–246.

Parpura V, Haydon PG, Henderson E. 1993. Three-dimensional imaging of living neurons and glia with the atomic force microscope. J Cell Sci 104 (Part 2):427–432.

Pesen D, Hoh JH. 2005. Micromechanical architecture of the endothelial cell cortex. Biophys J 88:670–679.

Ricci D, Grattarola M, Tedesco M. 2004. Growth cones of living neurons probed by atomic force microscopy. Methods Mol Biol 242:125–140.

Robles E, Woo S, Gomez TM. 2005. Src-dependent tyrosine phosphorylation at the tips of growth cone filopodia promotes extension. J Neurosci 25:7669–7681.

Rochlin MW, Dailey ME, Bridgman PC. 1999. Polymerizing microtubules activate site-directed F-actin assembly in nerve growth cones. Mol Biol Cell 10:2309–2327.

Rotsch C, Braet F, Wisse E, Radmacher M. 1997. AFM imaging and elasticity measurements on living rat liver macrophages. Cell Biol Int 21:685–696.

Santos NC, Castanho MA. 2004. An overview of the biophysical applications of atomic force microscopy. Biophys Chem 107:133–149.

Scalia F, Matsumoto DE. 1985. The morphology of growth cones of regenerating optic nerve axons. J Comp Neurol 231:323–338.

Schaefer AW, Kabir N, Forscher P. 2002. Filopodia and actin arcs guide the assembly and transport of two populations of microtubules with unique dynamic parameters in neuronal growth cones. J Cell Biol 158:139–152.

Schneider J, Dufrene YF, Barger WR Jr, Lee GU. 2000. Atomic force microscope image contrast mechanisms on supported lipid bilayers. Biophys J 79:1107–1118.

Schneider SW, Sritharan KC, Geibel JP, Oberleithner H, Jena BP. 1997. Surface dynamics in living acinar cells imaged by atomic force microscopy: Identification of plasma membrane structures involved in exocytosis. Proc Natl Acad Sci USA 94:316–321.

Sheiko SS, Moller M, Reuvekamp EM, Zandbergen HW. 1993. Calibration and evaluation of scanning-force-microscopy probes. Phys Rev B Condens Matter 48:5675–5678.

Song H, Poo M. 2001. The cell biology of neuronal navigation. Nat Cell Biol 3:E81–E88.

Suter DM, Errante LD, Belotserkovsky V, Forscher P. 1998. The Ig superfamily cell adhesion molecule, apCAM, mediates growth cone steering by substrate-cytoskeletal coupling. J Cell Biol 141:227–240.

Suter DM, Forscher P. 2001. Transmission of growth cone traction force through apCAM-cytoskeletal linkages is regulated by Src family tyrosine kinase activity. J Cell Biol 155:427–438.

Suter DM, Schaefer AW, Forscher P. 2004. Microtubule dynamics are necessary for SRC family kinase-dependent growth cone steering. Curr Biol 14:1194–1199.

Tojima T, Yamane Y, Takagi H, Takeshita T, Sugiyama T, Haga H, Kawabata K, Ushiki T, Abe K, Yoshioka T, Ito E. 2000. Three-dimensional characterization of interior structures of exocytotic apertures of nerve cells using atomic force microscopy. Neuroscience 101:471–481.

Wakatsuki T, Schwab B, Thompson NC, Elson EL. 2001. Effects of cytochalasin D and latrunculin B on mechanical properties of cells. J Cell Sci 114:1025–1036.

Williams RW, Borodkin M, Rakic P. 1991. Growth cone distribution patterns in the optic nerve of fetal monkeys: Implications for mechanisms of axon guidance. J Neurosci 11:1081–1094.

Wu DY, Goldberg DJ. 1993. Regulated tyrosine phosphorylation at the tips of growth cone filopodia. J Cell Biol 123:653–664.

Wu DY, Wang LC, Mason CA, Goldberg DJ. 1996. Association of β1 integrin with phosphotyrosine in growth cone filopodia. J Neurosci 16:1470–1478.

Xue Y, Honig MG. 1999. Ultrastructural observations on the expression of axonin-1: Implications for the fasciculation of sensory axons during axonal outgrowth into the chick hindlimb. J Comp Neurol 408:299–317.

Zhang XF, Schaefer AW, Burnette DT, Schoonderwoert VT, Forscher P. 2003. Rho-dependent contractile responses in the neuronal growth cone are independent of classical peripheral retrograde actin flow. Neuron 40:931–944.